Determination of k_B via Johnson-Nyquist Noise Measurements

Neil Ghugare

The Ohio State University, Department of Physics, Columbus, OH 43210

April 30, 2026

Abstract

The Boltzmann constant k_B defines the fundamental limit of signal sensitivity in electronic detectors by relating thermal energy to microscopic voltage fluctuations. In this experiment, we determined k_B by measuring Johnson-Nyquist noise as a function of resistance, bandwidth, and temperature. Using a high-gain amplification chain and variable Butterworth filters, we characterized the mean-square voltage fluctuations across a range of 1Ω to 10MΩ, and frequency spans up to ∼100 kHz. We isolated the thermal noise component by accounting for the intrinsic amplifier noise floor and utilized liquid nitrogen to verify the predicted linear dependence on absolute temperature down to 85K. Our analysis yielded an experimental value for k_B of $(1.39 \pm 0.02) \times 10^{-23}$ J/K within 0.5σ of the nominal value, demonstrating the robustness of the fluctuation-dissipation theorem in describing the noise limits of modern instrumentation, such as astronomical CCDs and detectors.

1 Introduction

The precise determination of fundamental physical constants is a cornerstone of modern metrology, linking theoretical frameworks to experimental reality. The Boltzmann constant k_B, in particular, bridges microscopic thermal energy and macroscopic temperature [1]. Following the 2019 SI redefinition, k_B is now a fixed value (1.380649×10^{-23} J/K) used to define the Kelvin [8]. Consequently, measurements of Johnson Noise now serve as a verification of thermodynamic consistency and a primary thermometry technique [1]. In electronic systems, this thermal energy manifests as spontaneous voltage fluctuations across resistive elements [1]. First observed by Johnson and theoretically explained by Nyquist, these fluctuations provide a direct pathway to measuring k_B through the fluctuation-dissipation theorem [1, 3].

Characterizing these fluctuations is a practical necessity for high-sensitivity instrumentation, particularly in observational astronomy. The performance of Charge-Coupled Devices (CCDs) is fundamentally limited by the thermal "noise floor" of readout electronics [5]. To achieve the signal-to-noise ratios required for detecting faint cosmic signals, these instruments are operated at cryogenic temperatures to suppress Johnson Noise [5].

In this report, we characterize Johnson Noise across varying resistances, bandwidths, and temperatures using a high-gain amplification system. By analyzing the linear relationship between mean-square noise voltage and these parameters, we determine an experimental value for k_B. Our results demonstrate the robustness of the Nyquist prediction and explore the limitations imposed by intrinsic amplifier noise.

2 Theory

The statistical mechanics of a conductor in thermal equilibrium predicts spontaneous voltage fluctuations rooted in the "electron gas" model [1]. Here, conduction electrons undergo random thermal motion where, according to the equipartition theorem, each degree of freedom possesses an average energy of $\frac{1}{2}k_{\mathrm{B}}T$ [1]. These fluctuations distribute energy across the electromagnetic modes of the conductor, resulting in a non-zero time-averaged power as described by Nyquist relation [1]:

$$\langle V_{\mathrm{J}}^2 \rangle = 4k_{\mathrm{B}}TR\Delta f, \tag{1}$$

where k_{B} is the Boltzmann constant, R is the resistance, T is the absolute temperature, and Δf is the effective frequency bandwidth. A derivation is provided in Supplement A.

In a physical measurement system, we must account for the intrinsic amplifier noise voltage $\langle V_{\mathrm{N}}^2 \rangle$ [1]. The composite signal undergoes two-stage amplification (total gain $G = G_1G_2$) and frequency filtering before reaching a "squarer" module. This module produces a time-averaged DC output, $\langle V_{\mathrm{sq}} \rangle$, related to the input noise by:

$$\langle V_{\mathrm{sq}} \rangle = \frac{(G_1G_2)^2}{10\ \mathrm{V}} \langle V_{\mathrm{J}}^2 + V_{\mathrm{N}}^2 \rangle, \tag{2}$$

where the 10 V is an internal scaling constant. By substituting Eq. into Eq.2, k_{B} can be isolated via linear regression of $\langle V_{\mathrm{sq}} \rangle$ against R, T, or Δf. Detailed filter responses and bandwidth characterizations are found in Supplement B.

3 Experimental Methods

Thermal voltage fluctuations were generated across a source resistor R housed in a shielded "Low Level Electronics" (LLE) box to mitigate electromagnetic interference [1]. As show in Fig. 1, these signals underwent a two-stage amplification process: an initial fixed-gain pre-amplifier ($G_1 = 600$) followed by a variable-gain main amplifier (G_2) used to scale the noise for the analog processing [1]. To isolate specific frequency components, we utilized high- and low-pass Butterworth filters. We characterized the effective noise bandwidth Δf by verifying corner frequencies with a function generator and oscilloscope, ensuring alignment with the predicted attenuation curves (Supplement B) [1, 2]. The processed signal was then integrated by a squarer module and recorded as a mean-square output on a digital multimeter using a 1-second time constant to average fluctuations [1].

We calibrated the system's intrinsic noise floor $\langle V_{\mathrm{N}}^2 \rangle$ by measuring the output at 1Ω and 10Ω and extrapolating to 0Ω. This baseline was subsequently subtracted from all measurements [1]. With the signal chain characterized, we performed three distinct measurement regimes: (i) varying R from 1Ω to 10 MΩ at constant T and Δf, (ii) varying Δf at constant R and T, and (iii) varying T by submerging resistors in liquid nitrogen. For cryogenic trials, we allowed the system to reach temperatures of ∼85K and recorded simultaneous resistance-temperature data to account for the temperature-dependent sensitivity of the source elements [1, 2].

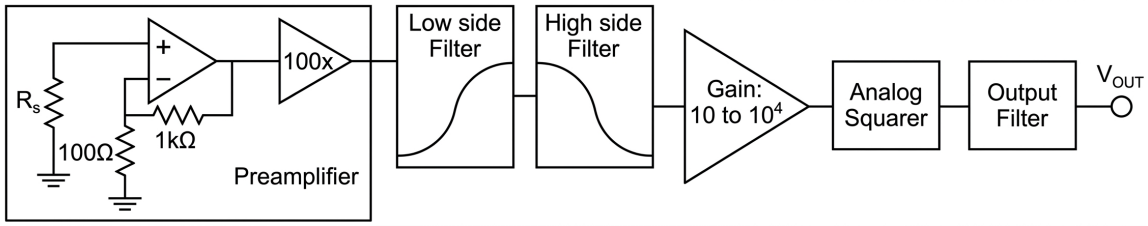

Figure 1: Block diagram of our apparatus [3]. In the low-level electronics box (LLE), we have a source resistor of choice R_S which goes into a preamplifier, which amplifies our signal by 600x [1]. Then, in the high-level electronics box (HLE), we can choose our bandwidth utilizing low- and high-side filters [1]. We can then adjust the gain manually to further amplify our signal, and it goes through an analog squarer and time-averaging output filter, outputting the squared voltage measurement to a digital multimeter [1].

4 Data Analysis and Results

For each measurement, we calculate the amplifier noise for the given bandwidth, and then use that with Eq. 2 to find $\langle V_J^2 \rangle$. Then we fit the linear segment to Eq. 1 to then extract k_B using an Orthogonal Distance Regression (ODR) fit with errors as detailed in Supplement C.

4.1 Johnson Noise vs. Resistance Analysis

We analyzed Johnson Noise vs. Resistance for two fixed bandwidths, 0.1-100.0 kHz and 1.0-10.0 kHz, as shown in Fig. 2. We verified the linear dependence of Johnson Noise on R by measuring the mean-square output voltage for resistors ranging from 1Ω to 10MΩ, at a fixed T of 295.4 K. This linear proportionality confirms the Nyquist prediction that this thermal noise power is proportional to resistance [1]. The weighted-average fit on the linear data, with errors as in Supplements C.1 and C.4, yielded a k_B value of $(1.39 \pm 0.04) \times 10^{-23}$ J/K, within 0.25σ and within 0.7% error of the nominal value of 1.38×10^{-23} J/K [1]. The reduced χ^2 values of 0.91 and 0.87 indicate a good fit to the data with well-propagated errors.

The Nyquist model (Eq. 1) assumes an ideal resistor. However, experimental constraints impose a "sweet spot" for accurate measurements. At low resistances ($R < 100\Omega$), the signal is dominated by the intrinsic amplifier noise floor [1]. Conversely, at extremely high resistances, parasitic capacitance within the circuit creates a filtering effect that attenuates the high-frequency components of the Johnson Noise [1]. To minimize these distortions, we utilized mid-range resistors (10 kΩ) for our subsequent bandwidth and temperature trials, ensuring the validity of the linear approximation.

4.2 Johnson Noise vs. Bandwidth Analysis

We analyze Johnson Noise vs. Bandwidth for a fixed T of 295.4 K and R of 10 kΩ, as shown in Fig. 3. We measured for ENBW values ranging from 1000 Hz to 110,961 Hz. We verified the linear dependence of the squared voltage on bandwidth [1]. The fit on the data with errors yielded a k_B value of $(1.40 \pm 0.02) \times 10^{-23}$ J/K, withing 1σ and within 1.4% of the nominally accepted value [1]. The reduced χ^2 of 5.10 indicates a good fit of the data, but also likely indicates an underestimation of our errors.

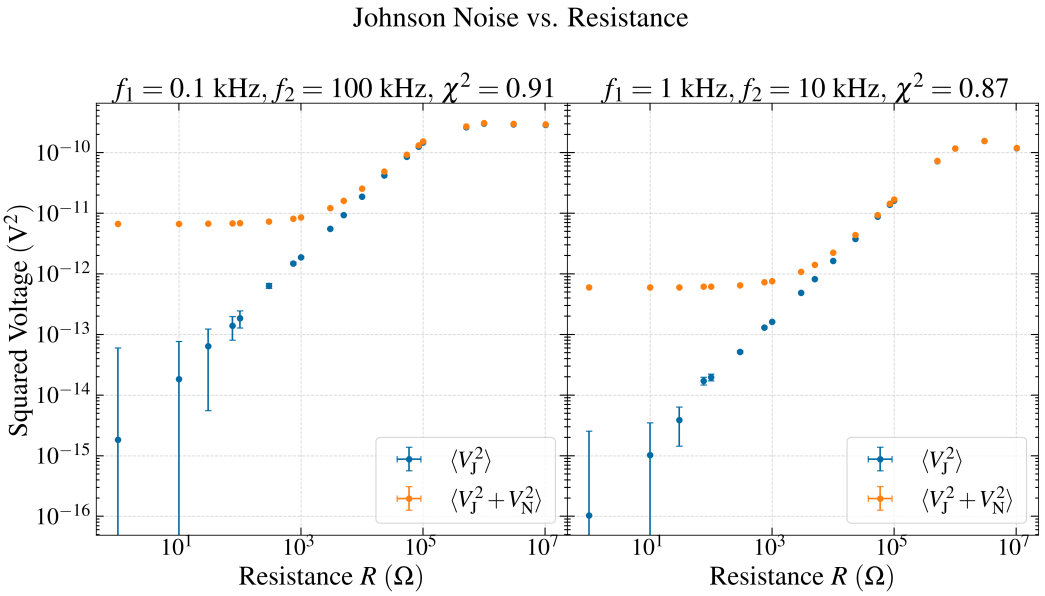

Figure 2: Johnson Noise vs. Resistance (1Ω-10MΩ) with a fixed T of 295.4 K and fixed Δf of 0.1-100 kHz (left) and 1-10 kHz (right). Raw measurements (orange) are corrected for intrinsic amplifier noise (blue) to extend the linear regime [2]. Linear regressions yield a k_B value of $(1.40 \pm 0.06) \times 10^{-23}$ J/K and $(1.38 \pm 0.06) \times 10^{-23}$ J/K, respectively. The reduced χ^2 values are 0.91 and 0.87, respectively, indicating a good fit to the data and well-estimated errors. A weighted average yields a k_B value of $(1.39 \pm 0.04) \times 10^{-23}$, falling within 0.25σ and within 0.7% error of the nominally accepted value [1].

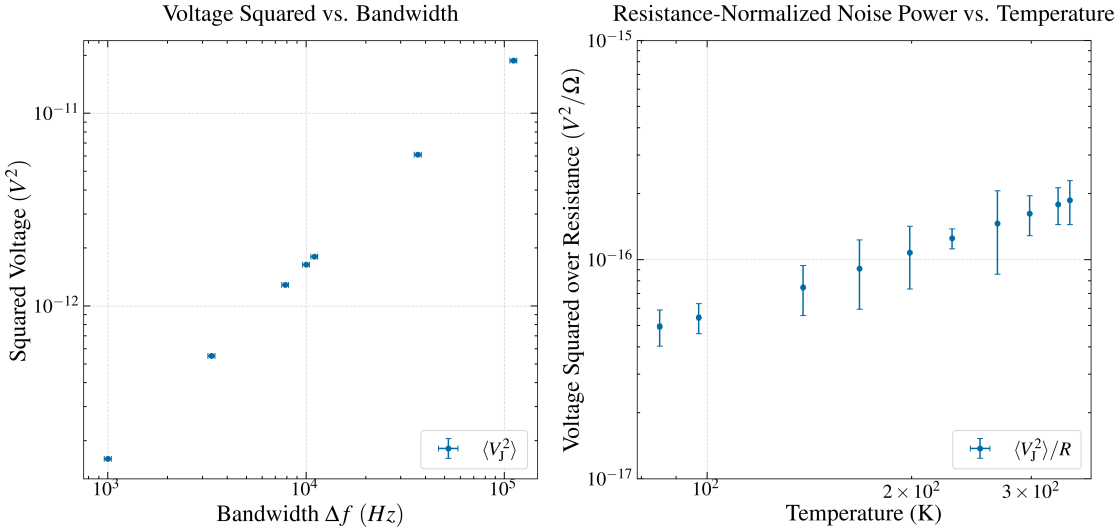

Figure 3: Plot of Johnson Noise vs. Bandwidth (left) and Johnson Noise/Resistance vs. Temperature (right) for R = 10kΩ. For bandwidth trials, Δf ranged from 1000-110,961 Hz, with a fixed T of 295.4 K. Fitting yielded a k_B value of $(1.40 \pm 0.02) \times 10^{-23}$ J/K, within 1σ of the nominally accepted value [1]. The fit returned a reduced χ^2 of 5.10, indicating an underestimation of our errors, likely stemming from unmodeled cable capacitance and amplifier roll off, discussed in Sec. 5. For the temperature plot, we used a fixed Δf of 9997 Hz, with the submerged 10Ω resistor calibrating the amplifier noise. Fitting yielded a k_B value of $(1.38 \pm 0.05) \times 10^{-23}$ J/K, agreeing with the accepted value of 1.38×10^{-23} J/K [1]. The fit returned a reduced χ^2 of 0.3, indicating overestimated errors, likely from large σ_T.

4.3 Johnson Noise vs. Temperature Analysis

Finally, we analyzed the relationship between Johnson Noise and temperature for a fixed Δf of 9997 Hz and R of 10 kΩ, for T ranging from 85-342K, as shown in Fig. 3. Because the resistance of the source element is not constant with T, we analyzed the squared voltage over the resistance $\langle V_J^2 \rangle / R$ [2]. This ensures that any observed change in noise power is a direct consequence of thermal energy rather than a shift in the resistance. As predicted by Eq. 1, the normalized noise power exhibited a linear dependence on temperature. Fitting to the data with errors in Supplements C.3 and C.4 yielded a k_B value of $(1.38 \pm 0.05) \times 10^{-23}$ J/K, within the nominally accepted value [1]. The reduced χ^2 for the fit was 0.3, indicating some overestimated errors.

5 Discussion and Conclusions

A weighted average of all experimental regimes yields $k_B = (1.39 \pm 0.02) \times 10^{-23}$ J/K, in agreement with the nominal value within 0.5σ [1]. The resistance measurements provided the most robust determination ($\chi^2 \approx 1$), while the higher χ^2 (5.10) in the bandwidth trial suggest systematic underestimation of errors. This discrepancy likely stems from the parasitic capacitance of the coaxial cables which, as explored in prior studies of pulse transmission, acts as an additional low-pass filter in parallel with the source resistor [1]. This effect attenuates noise power at high frequencies, distorting the linear Δf relationship [1]. Additionally, while cryogenic trials successfully isolated the linear T dependence of Eq. 1, stability of the LN_2 thermal equilibrium limited precision.

Statistical uncertainties remain constrained by the Dicke Limit, where the stochastic nature of the signal requires long integration times to achieve high precision [1]. Future improvements, such as automated high-frequency sampling and increased averaging times, could further suppress these fluctuations. Systematic constraints were dominated by resistor tolerances and the intrinsic amplifier noise floor. Despite these limits, our results verify that Johnson Noise is an inescapable thermodynamic constraint. This displays the necessity of cryogenic cooling in high-sensitivity instrumentation, such as CCDs, to suppress thermal noise below the detection threshold for faint signals [5]. Finally, our results confirm that accurate measurements require operating within a "sweet spot" of resistance; mid-range R values avoid the dominance of the amplifier noise floor at low R and the capacitive effects at high R [1].

References

[1] Noise Fundamentals NF1-A Instructor's Manual, TeachSpin Inc., (2010).

[2] READ ME Hints for Johnson Noise Experiment, Carmen/Canvas, (2026).

[3] Noise Fundamentals Conceptual Introduction, Carmen/Canvas, (2026).

[4] Kittel, Charles. Elementary Statistical Physics, (Robert E. Krieger, 1988), Chap 29.

[5] Howell, Steve B. Handbook of CCD Astronomy, (Cambridge University Press, 2006).

[6] Zoyi Electronic Technology Co., Ltd., ZT111 Digital Multimeter User Manual, (2018), p. 21. Available: https://www.manualslib.com/manual/1522469/Zotek-Zt111.html?page=25#manual.

[7] B&K Precision Corp., 4 1/2 Digit and 50,000 Count Bench Multimeters USER MANUAL, (2010). https://assets.testequity.com/te1/Documents/pdf/bk/2831E-5491B_manual.pdf

[8] Bureau International des Poids et Mesures (BIPM), The International System of Units (SI), 9th ed. (BIPM, Sèvres, 2019).

Supplement

A Johnson-Nyquist Derivation

A.1 Introduction

The Johnson-Nyquist theorem, the cornerstone of this paper, provides a quantitative expression for the thermal noise generated by a system in equilibrium [4]. Multiple derivations exist, like those based on 1D transmission line modes, but this supplement focuses on a microscopic argument that links the random motion of charge carries directly to the observed mean square voltage, as in *Elementary Statistical Physics* by Charles Kittel [4].

A.2 The Microscopic Model

Consider a resistor of resistance R with N electrons per unit volume, length l and a cross-sectional area A [4]. The electrons are treated as a Maxwellian gas, where the average thermal energy per degree of freedom is governed by the classical equipartition theorem [4]

$$\frac{1}{2}m\bar{v}^2 = \frac{1}{2}k_{\mathrm{B}}T \Rightarrow \overline{v^2} = \frac{k_{\mathrm{B}}T}{m}, \tag{A.1}$$

where v represents the random velocity component of an electrong along the axis of the resistor [4].

A.3 Voltage and Velocity Correlation

The total voltage V across the resistor is the sum of the random voltage contributions V_i from each individual electron [4],

$$V = \sum_i V_i = \left(\frac{Re}{l}\right)\sum_i v_i. \tag{A.2}$$

We note that the spectral density function $G(f)$ has the property that in the range of an effective noise bandwidth Δf [4]:

$$\overline{V_i^2} = G(f)\Delta f. \tag{A.3}$$

To determine the spectral density $G(f)$, we define a correlation function $C(\tau)$ based on the carrier relaxation time τ_{c} (the mean time of flight) [4]:

$$C(\tau) = \overline{V_i(t)V_i(t+\tau)} = \overline{V_i^2}e^{-\tau/\tau_{\mathrm{c}}}. \tag{A.4}$$

A.4 Application of the Wiener-Khintchine Theorem

Using the Wiener-Khintchine theorem to relate the correlation function to the frequency domain, the spectral density is expressed as [4]:

$$G(f) = 4\left(\frac{Re}{l}\right)^2 \overline{v^2} \frac{\tau_c}{1+(2\pi f \tau_c)^2}. \tag{A.5}$$

In typical conductors, the relaxation time τ_c is extremely small (approximately 10^{-13} sec), allowing the denominator term $(2\pi f \tau_c)^2$ to be neglected for frequencies through the microwave range [4].

A.5 Final Derivation

From Eq. A.3, we can find the mean square voltage:

$$\overline{V_i^2} = G(f)\Delta f = 4\left(\frac{Re}{l}\right)^2 \overline{v^2} \frac{\tau_c}{1+(2\pi f \tau_c)^2} \Delta f. \tag{A.6}$$

Substituting the thermal velocity $\overline{v^2} = k_B T/m$ [4]:

$$\overline{V_i^2} = 4\left(\frac{Re}{l}\right)^2 \left(\frac{k_B T}{m}\right) \frac{\tau_c}{1+(2\pi f \tau_c)^2} \Delta f. \tag{A.7}$$

To get from $\overline{V_i^2}$ to $\overline{V^2}$, we use a modification of Eq. A.2,

$$\overline{V^2} = \sum_i \overline{V_i^2} = \overline{V_i^2} \cdot N_{\text{total}},$$

where N_{total} is the total number of electrons given by NAl [4]. Hence,

$$\overline{V^2} = NAl \cdot 4\left(\frac{Re}{l}\right)^2 \left(\frac{k_B T}{m}\right) \frac{\tau_c}{1+(2\pi f \tau_c)^2} \Delta f. \tag{A.8}$$

Rearranging this, we see that

$$\overline{V^2} = (4k_B T R \Delta f)\left(\frac{NAlRe^2\tau_c}{ml^2}\right) = (4k_B T R \Delta f)\left(\frac{Ne^2\tau_c}{m}\right)\left(\frac{RA}{l}\right). \tag{A.9}$$

To simplify this relation, we introduce the concept of electrical conducitivity σ, where [4]

$$\sigma = \frac{l}{RA} = \frac{Ne^2\tau_c}{m}. \tag{A.10}$$

Thus, we can rewrite Eq. A.9 to yield

$$\overline{V^2} = (4k_{\mathrm{B}}TR\Delta f)(\sigma)\left(\frac{1}{\sigma}\right).$$

So, we yield the Johnson-Nyquist relation:

$$\boxed{\overline{V^2} = \langle V_{\mathrm{J}}^2 \rangle = 4k_{\mathrm{B}}TR\Delta f.}$$

The derivation for the electrical conductivity equations can be taken for granted, or derived using the drift velocity equation, as done by Kittel [4]. Likewise, after this result, Kittel discusses the Maxwellian assumption and shows how it has no effect on the noise power [4].

B Butterworth Filters and Verification

Given the Johnson-Nyquist equation

$$\langle V_{\mathrm{J}}^2 \rangle = 4k_{\mathrm{B}}TR\Delta f, \tag{B.1}$$

the bandwidth Δf is the *effective noise bandwidth (ENBW)* [1]. Table 1.5 in the manual gives these values for various high- and low-pass filter values [1]. These values are not simply $f_2 - f_1$, and this is due to the fact that theory assumes that filter band-passes work as a "brick wall" model, where the filter response is 1 for a frequency f for $f_1 < f < f_2$ and 0 otherwise [1]. However, real-world filters work via the "Butterworth model", where the filter response gradually declines at the corner frequency [1]. Table 1.5 gives these values for a given bandwidth, and we verify these results for multiple bandwidths to feel comfortable in using the table as-is [1]. We verify for four bandwidths: 0.1-1.0 kHz, 0.1-100.0 kHz, 3.0-100.0 kHz, and 1.0-10.0 kHz. Using a function signal generator, we vary our frequency values, and we measure the RMS voltage in and the RMS voltage out from the high-level electronics box. We can then measure the gain $G(f)$ through

$$G(f) = \frac{V_{\text{rms, out}}}{V_{\text{rms, in}}}. \tag{B.2}$$

We plot $G(f)$ vs. f and then fit it to theoretical prediction [1, 2]:

$$G(f) = \left\{ (f/f_1)^2 \left[1 + (f/f_1)^4 \right]^{-1/2} \right\} \left\{ \left[1 + (f/f_2)^4 \right]^{-1/2} \right\}. \tag{B.3}$$

Plots for our bandwidths with the theoretical model and model fitting is shown in Figs. B.1 to B.4.

We then numerically check the ENBW value for Δf utilizing the definition [1],

$$\text{ENBW} = \int_0^\infty G^2(f)\, df, \tag{B.4}$$

where $G^2(f)$ utilizes the f_1 and f_2 values from the fit of our data to Eq. B.3. This is done numerically on the fit through trapezoidal approximation for integration. We tabulate our results in Table B.1, confirming our ability to use Table 1.5 in the manual.

f_1 (kHz)	f_2 (kHz)	Δf (Exp.)	Δf (Table 1.5) [1]	% Error
0.1	1.0	1,004	1,000	0.4%
0.1	100.0	115,091	110,961	3.7%
3.0	100.0	112,592	107,740	4.3%
1.0	10.0	10089	9997	0.9%

Table B.1: Tabulated values for our Δf ENBW value (Exp.) and the comparison with Table 1.5 in the manual, with percent error. The manual states that all computed values in Table 1.5 are subject to uncertainties of order 4% [1]. We see that all our values fall within this threshold, except for that of the 3.0-100.0 kHz bandwidth. The manual also states that the column including this 3.0-100.0 kHz bandwidth is computed ignoring systematic effects, which may increase the values by $3 \pm 1\%$ and that there are further corrections for large f_2 values [1]. Since the 3.0-100.0 kHz bandwidth is the bottom right corner of Table 1.5, it is susceptible to these effects, likely accounting for the uncertainty being larger than the nominal 4% uncertainty [1].

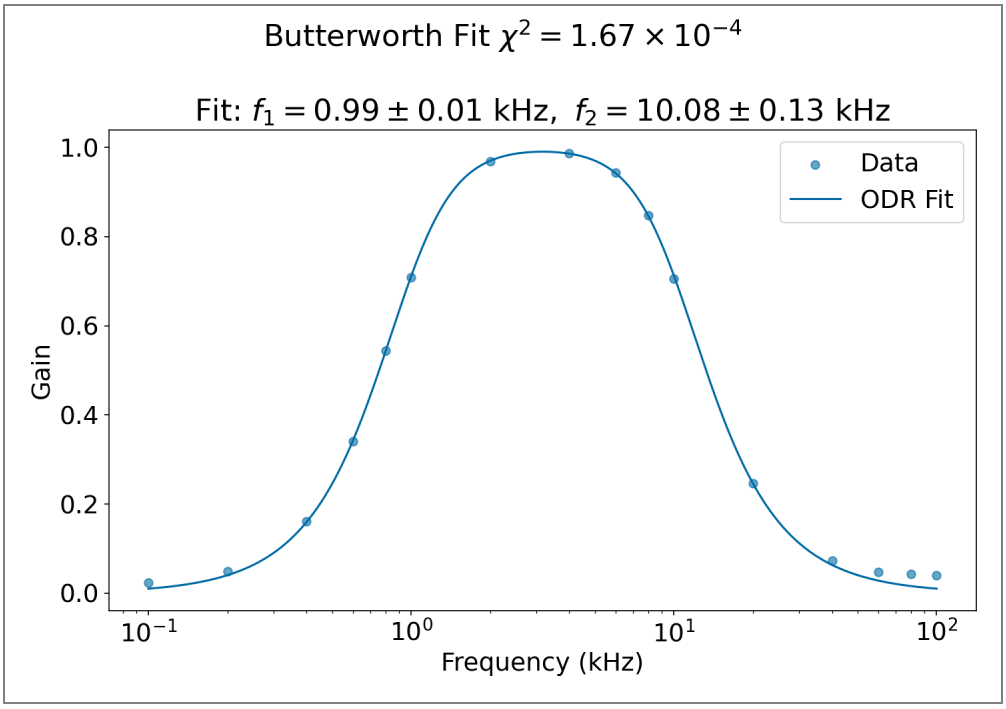

Figure B.1: Numerical Butterworth fit of Eq. B.3 to the 1.0-10.0 kHz bandwidth. The fit returned extracted band-pass values of $f_1 = 0.99 \pm 0.01$ kHz and $f_2 = 10.08 \pm 0.13$ kHz, both within 1σ of the expected bandwidth value. Numerically integrating $G^2(f)$ over f yields an ENBW value of 10,088, a 0.9% error from the nominally calculated value of 9,997 [1]. This is within the known uncertainty of the nominal value of 4% [1].

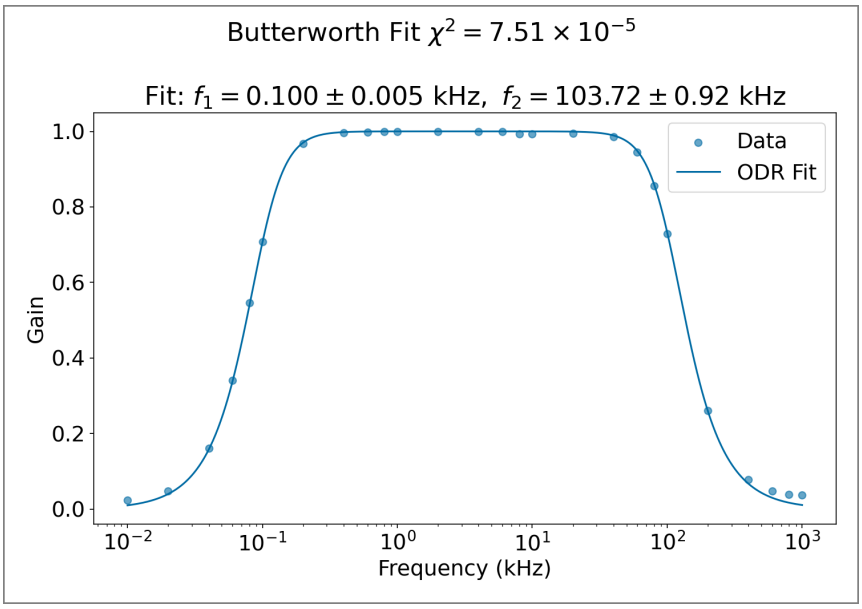

Figure B.2: Numerical Butterworth fit of Eq. B.3 to the 0.1-100.0 kHz bandwidth. The fit returned extracted band-pass values of $f_1 = 0.100 \pm 0.005$ kHz and $f_2 = 103.72 \pm 0.92$ kHz, within 1σ and 4.04σ. The $\sim 4\sigma$ deviation for f_2 can be explained by the systematic error on the high-end frequency, causing deviation in the fit. These effects cause fluctuations in the RMS voltage and calculated G, likely caused by high-frequency peaking or parasitic inductance. Numerically integrating $G^2(f)$ over f yields an ENBW value of 115,091, a 3.7% error from the nominally calculated value of 110,961 [1]. This is within the known uncertainty of the nominal value of 4% [1].

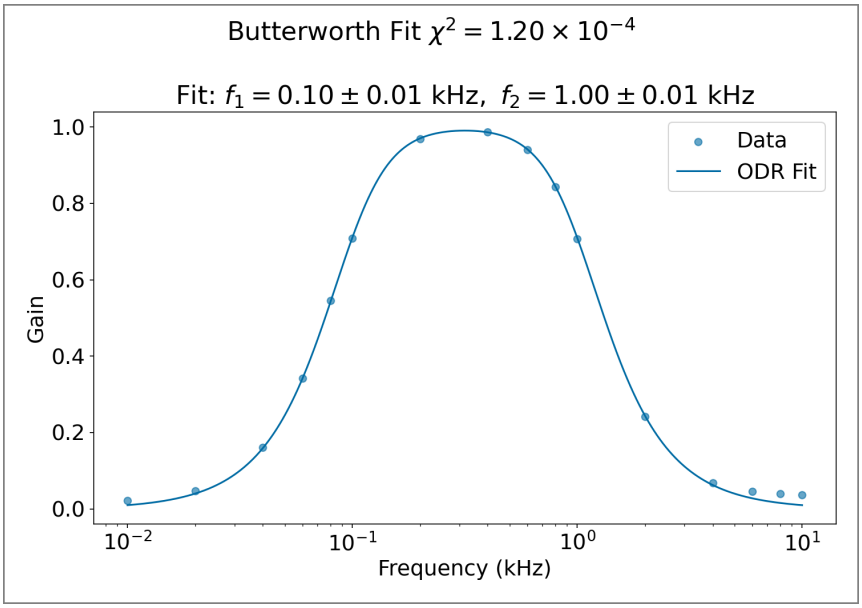

Figure B.3: Numerical Butterworth fit of Eq. B.3 to the 0.1-1.0 kHz bandwidth. The fit returned extracted band-pass values of $f_1 = 0.10 \pm 0.01$ kHz and $f_2 = 1.00 \pm 0.01$ kHz, both within 1σ of the expected bandwidth value. Numerically integrating $G^2(f)$ over f yields an ENBW value of 1004, a 0.4% error from the nominally calculated value of 1,000 [1]. This is within the known 4% uncertainty of the nominal value [1].

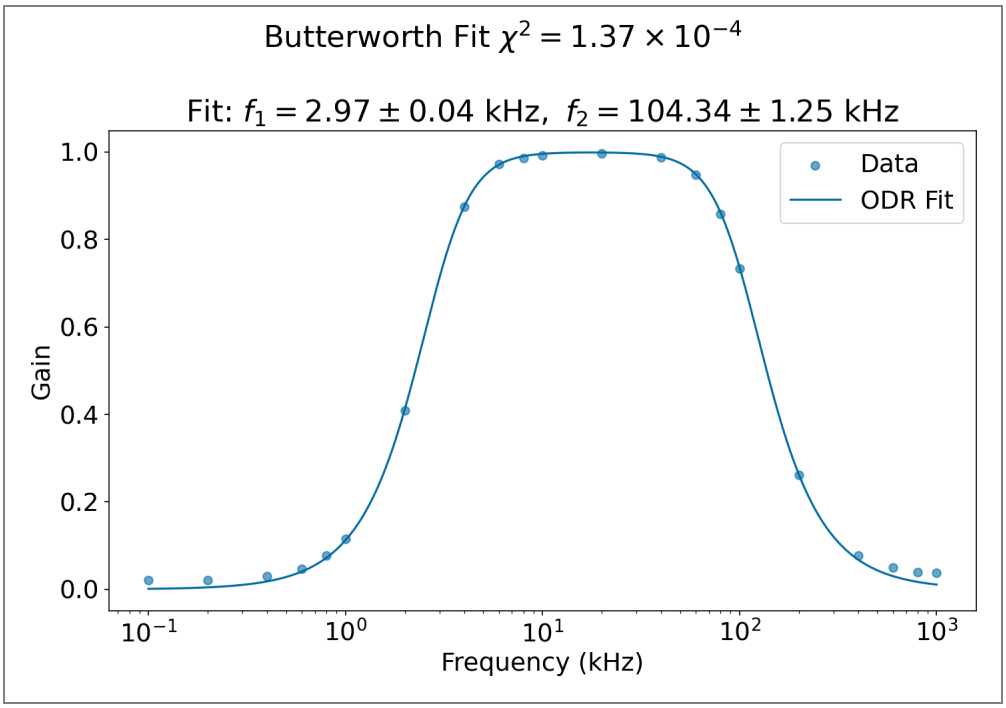

Figure B.4: Numerical Butterworth fit of Eq. B.3 to the 3.0-100.0 kHz bandwidth. The fit returned extracted band-pass values of $f_1 = 2.97 \pm 0.04$ kHz and $f_2 = 104.34 \pm 1.25$ kHz, within 1σ and 3.47σ. The $\sim 3.5\sigma$ deviation for f_2 can be explained by the systematic error on the high-end frequency, causing deviation in the fit. These effects cause fluctuations in the RMS voltage and calculated G, likely caused by high-frequency peaking or parasitic inductance. Numerically integrating $G^2(f)$ over f yields an ENBW value of 112,592, a 4.4% error from the nominally calculated value of 107,740 [1]. This is more than the nominal uncertainty of 4%, but the nominal value doesn't include systematic effects and further corrections for large f_2 values, accounting for the discrepancy [1].

C Error Propagation and Analysis

C.1 Resistance Errors

For the Johnson Noise vs. Resistance measurement, we use errors in the Johnson Noise and errors in the resistance for the ODR fits. The resistance error for the resistors built into the low-level electronic (LLE) is subject to the manufacturer's 1% tolerance [1]. The resistors added to the LLE box are subject to errors by the Zotek ZT111 multimeter used to measure the resistance values, given by Table C.1 [6].

Range	Resolution	Accuracy
99.99Ω	0.01Ω	$\pm(1.0\% + 3)$
999.9Ω	0.1Ω	$\pm(0.5\% + 3)$
9.999kΩ	0.001kΩ	$\pm(0.5\% + 3)$
99.99kΩ	0.01kΩ	$\pm(0.5\% + 3)$
999.9kΩ	0.1kΩ	$\pm(0.5\% + 3)$
9.999MΩ	0.001MΩ	$\pm(1.5\% + 3)$
99.99MΩ	0.01MΩ	$\pm(1.5\% + 3)$

Table C.1: Resistance errors given by the Zotek ZT111 multimeter [6]. The error bars in resistance are then given by the accuracy column, with the percentage being the percentage of the measured value, and the $+3$ being the number of counts of resolution to add to the error [6].

The errors in the Johnson Noise measurement itself is an error added in quadrature from: a) the standard deviation of multiple measurements of the noise for one resistance, temperature, and bandwidth, and b) the error in measurement of the BK Precision 2831E multimeter. The error in the multimeter is given by the following formula, since our operating voltage range is less than 2 V [1, 7]:

$$\sigma_{2831\text{E}} = (0.03\% \text{ measurement}) + 0.0105 \text{ V}. \tag{C.1}$$

Eq. C.1 is given by the 2831E manual's error of 0.03% measurement + 0.05% range [7]. Since the range is the same for our entire array of voltage measurements, we get a fixed range error of 0.0105 V [7]. Hence, our Johnson Noise errors, if σ_{meas} is the standard deviation of the measured noise values, is given by

$$\sigma_{\text{noise}} = \sqrt{\sigma_{2831\text{E}}^2 + \sigma_{\text{meas}}^2}. \tag{C.2}$$

C.2 Bandwidth Errors

For the Johnson Noise vs. Bandwidth measurement, we use errors in the Johnson Noise and errors in the bandwidth for the ODR fits. After successful verification of the effective noise bandwidth values in Supplement B, we are comfortable using the values in Table 1.5 of the manual [1]. The

values for the ENBW (Δf) are subject to errors of 4% [1]. For errors in the Johnson Noise, we have the same error propagation as in Supplement C.1 and Eq. C.2.

C.3 Temperature Errors

For the Johnson Noise vs. Temperature measurement, we use errors in the Johnson Noise and errors in the temperature for the ODR fits. The errors in the temperature are given by fluctuations in the voltage measurement that monotonically relates to the temperature [1]. We take this to be 1 K for all measurements, which is a voltage fluctuation of about 1 mV. The errors in the noise itself come from the same propagation as in Supplement C.1 and Eq. C.2.

C.4 Boltzmann Constant Errors

Given the Johnson-Nyquist relation,

$$\langle V_{\mathrm{J}}^2 \rangle = 4 k_{\mathrm{B}} T R \Delta f, \tag{C.3}$$

we can rearrange and see that

$$k_{\mathrm{B}} = \frac{\langle V_{\mathrm{J}}^2 \rangle}{4 T R \Delta f}. \tag{C.4}$$

Hence, by propagation of errors using relative error method, we can find the uncertainty on k_{B} through

$$\sigma_{k_{\mathrm{B}}} = k_{\mathrm{B}} \sqrt{\left(\frac{\sigma_{\langle V_{\mathrm{J}}^2 \rangle}}{\langle V_{\mathrm{J}}^2 \rangle}\right)^2 + \left(\frac{\sigma_T}{T}\right)^2 + \left(\frac{\sigma_R}{R}\right)^2 + \left(\frac{\sigma_{\Delta f}}{\Delta f}\right)^2}, \tag{C.5}$$

with errors outlined in the previous sections. Note here that k_{B} in Eq. C.5 is the *experimental* k_{B} (Eq. C.4), not the nominal value.

If given some slope measurement from our ODR fitting process, this equation can be simplified. For example, for Johnson Noise vs. Resistance, if m is the slope representing $\langle V_{\mathrm{J}}^2 \rangle / R$, then the error propagation is simply

$$\sigma_{k_{\mathrm{B}}} = k_{\mathrm{B}} \sqrt{\left(\frac{\sigma_m}{m}\right)^2 + \left(\frac{\sigma_T}{T}\right)^2 + \left(\frac{\sigma_{\Delta f}}{\Delta f}\right)^2}. \tag{C.6}$$

We can repeat this process when bandwidth or temperature is the independent variable.